





Optical properties of InGaN-based red quantum well and microcavity

XIN HOU,¹ JIA-CONG GUO,¹ LI-LONG MA,¹ TAO YANG,¹
DAISUKE IIDA,^{2,5}  ZHAN SU,³ YANG MEI,¹  LEI-YING YING,¹
GUO-EN WENG,³  SHAO-QIANG CHEN,³  BAO-PING ZHANG,^{1,4,6}
AND KAZUHIRO OHKAWA²

¹Laboratory of Micro/nano-Optoelectronics, Department of Microelectronics and Integrated Circuits, Xiamen University, Xiamen 361005, China

²Computer, Electrical and Mathematical Sciences and Engineering (CEMSE) Division, King Abdullah University of Science and Technology (KAUST), Thuwal 23955-6900, Saudi Arabia

³State Key Laboratory of Precision Spectroscopy, Department of Electronic Engineering, East China Normal University, 500 Dongchuan Road, Shanghai 200241, China

⁴Institute of Nanoscience and Applications, Southern University of Science and Technology, Shenzhen 518055, China

⁵daisuke.iida@kaust.edu.sa

⁶bzhang@xmu.edu.cn

Abstract: Optical properties of InGaN/GaN red quantum well(QW) and their microcavities were studied and compared under optical pumping. Incidence of the excitation laser from the p-side was employed for both structures in order to acquire better emission characteristics. The QW structure was grown on sapphire substrate by metalorganic vapor-phase epitaxy(MOVPE) with a blue pre-layer QW. X-ray and scanning transmission electron microscopy(STEM) measurements demonstrate the good crystalline quality. Emissions from both blue and red QWs were observed and demonstrated to be dominated by radiative recombination. For red InGaN microcavity with two dielectric distributed Bragg reflector(DBR) mirrors, a high Q factor of 2355 at the longitudinal mode of 612.3 nm was achieved. Discrete higher-order modes were also clearly observed, being attributed to the lateral confinement on the photons in the microcavity caused by change in the refractive index of the laser-irradiation area because of the increase of carrier density. The Purcell effect accelerates the radiation recombination rate, leading to the fast decay process in the red InGaN microcavity which does exist for QWs only. Compared with the red QW sample, the emission of red microcavities is much purer and more stable. The above results lay a foundation for the realization of InGaN-based red vertical-cavity surface-emitting lasers(VCSELs) in the future.

© 2025 Optica Publishing Group under the terms of the [Optica Open Access Publishing Agreement](#)

1. Introduction

It is well-known that some challenges exist in high-indium-content InGaN/GaN QW including a large lattice mismatch [1], the quantum-confined Stark effect(QCSE) [2], phase separation [3], and the degradation of the crystal quality [4]. With the redshift of emission wavelength, that is, the increasing In content in the InGaN QW, the above problems become further serious [5]. It affects significantly the quality of the epitaxial wafer, and consequently the performance of related device as well.

In 1940, Edward Mills Purcell discovered the Purcell effect [6], which implies that the spontaneous emission(SE) rate of a material placing in a microcavity can be enhanced or suppressed depending on the optical density of states. When the SE rate is enhanced, the lifetime of carriers is rapidly reduced in the cavity [7]. The Fabry-Perot(FP) microcavity is one of the most familiarly optical microcavities. FP microcavity can improve the emission directivity and

the recombination efficiency of carriers. Firstly, the emission direction with a microcavity can be more focused and the divergence degree is reduced, which is conducive to improving the half-width, both in direction and in spectrum of the emission, and facilitating the integration of devices [8,9]. Secondly, the Purcell effect in high-quality microcavity leads to the increase of the SE rate and the emission intensity [7,10]. Simultaneously, high-quality microcavity is also a foundation for realizing high-performance optoelectronic devices, such as resonant cavity light emitting diodes(RCLEDS) and VCSELs and so on.

The problems in InGaN QW with high In content result in the larger blueshift and broadening of emission peak with increasing of injected carrier density. In addition, the large lattice mismatch and the degradation of the crystal quality in high-In-content QW sharply increases the intracavity loss, which weakens the energy storage capacity in the microcavity, as reflected by a low Q factor, and further deteriorates the optical performance of microcavity. At present, red RCLEDs based on GaN:Eu, O and AlInGaP have been reported, possessing Q values of 84 and 45, respectively [11,12]. There is only one report of orange-red InGaN based RCLEDs from our group, where the highest Q value is about 3010 at wavelength of 602 nm [13]. Therefore, it is urgent to expand research on this topic, in especially the design and fabrication of high-quality red InGaN microcavity, and the study of their optical properties.

In this work, a red InGaN single QW epitaxial structure was used to fabricate red microcavity. First, the optical properties of the red InGaN QW were investigated. And by STEM, the thicknesses of epitaxial layers were measured. We fabricated a red InGaN microcavity with emission wavelength 612.3 nm and Q value of 2355. It is shown that, by adopting a cavity, the blue shift and broad emission associated with QW can be significantly improved. Furthermore, by Photoluminescence(PL) and time resolved PL(TRPL)measurements, the different optical properties and carrier dynamics of the red InGaN QW and microcavity were investigated.

2. Epitaxial characterization and microcavity fabrication

Figure 1 shows the cross-sectional schematic of the red InGaN wafer structure grown on a patterned c-plane sapphire substrate by MOVPE. One 2.5 nm single blue QW and one 3 nm single red QW made up the InGaN active region. $\text{In}_{0.02}\text{Ga}_{0.98}\text{N}(11\text{ nm})/\text{Al}_{0.13}\text{Ga}_{0.87}\text{N}(18\text{ nm})/\text{GaN}(5\text{ nm})$ was used as a barrier structure between the two QWs. Using the $\text{In}_{0.02}\text{Ga}_{0.98}\text{N}$ layer as part of the barrier layer can reduce the lattice mismatch between the red InGaN well layer and the barrier layer. On the other hand, the $\text{Al}_{0.13}\text{Ga}_{0.87}\text{N}$ barrier layer between blue and red QW can suppress the carrier escape and injection into the blue QW because of the larger bandgap of $\text{Al}_{0.13}\text{Ga}_{0.87}\text{N}$. The 8- μm n-GaN buffer layer and the 30-layer superlattice were adopted to reduce the residual stress from underlayers [14,15]. The thin epitaxial structure of p-side is very beneficial to the emission output of the red microcavity. The detailed analysis will be given in the later discussion of half cavity.

The wafer structure was examined by STEM, as shown in Fig. 2. The measured results of the actual growth thickness in p-GaN and active region are consistent with the designed epitaxial structure parameters. The actual distance from red InGaN QW to the p-side surface is 133.94 nm. This result is helpful to accurately design the thickness and pairs of p-side DBRs. Meanwhile, the clear interface between layers and no defects and dislocations are observed in the STEM figure. These results indicate the good quality of the material.

The elemental mappings of Al, N, Ga and In atoms distributed in the InGaN active region were also measured by energy-dispersive X-ray spectroscopy(EDS), as shown in Fig. 3(a-e). In Fig. 3(e), it is clearly observed that the In content between the red QW and blue QW are significantly different. Meanwhile, the distribution of In elements in QWs is quite uniform, and no obvious segregation and accumulation. These results demonstrate again the good crystal quality of QWs and the successful control of the stress.

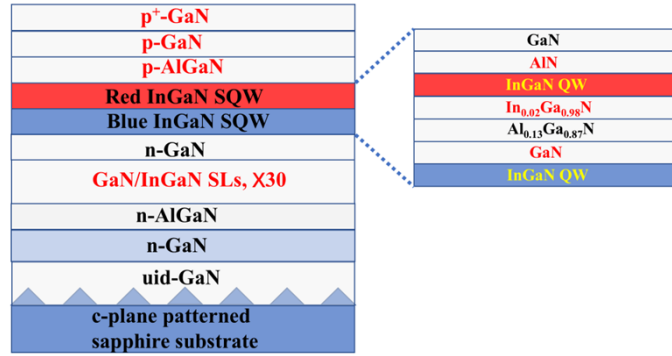


Fig. 1. Cross-sectional schematic of red InGaN-based wafer structure.

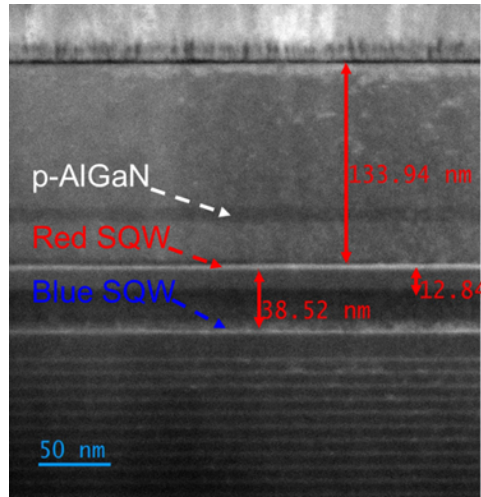


Fig. 2. The STEM of the QW wafer.

The excitation-energy-dependent PL measurements were carried out at 3.3 K, and the PL spectra are shown in Fig. 4(a). With increasing excitation energy, the blue shift of red peak is about 26 meV. The change of peak wavelength and full width at half maximum (FWHM) with different excitation energies are revealed in Fig. 4(b). At low excitation energy, the decrease of FWHM is mainly attributed to the screening of QCSE in red InGaN QW. With increasing excitation energy, the band filling effect leads to a slight broadening in FWHM of red peak as shown in Fig. 4(d) [13,15]. The integrated PL intensity (I) as a function of the excitation energy (E) can be expressed by the following equation [16]:

$$I \propto E^F \quad (1)$$

when $F = 1$, radiative recombination is dominated. As shown in Fig. 4(d), the F value of red peak is 0.825. Due to the relatively low growth temperature, the QW with high In content may cause degradation of the crystal quality, leading to consumption of photogenerated carriers by the defects. It is also true that Auger recombination caused by many body effects is usually expected under high carrier densities. However, from the variation of PL intensity as a function

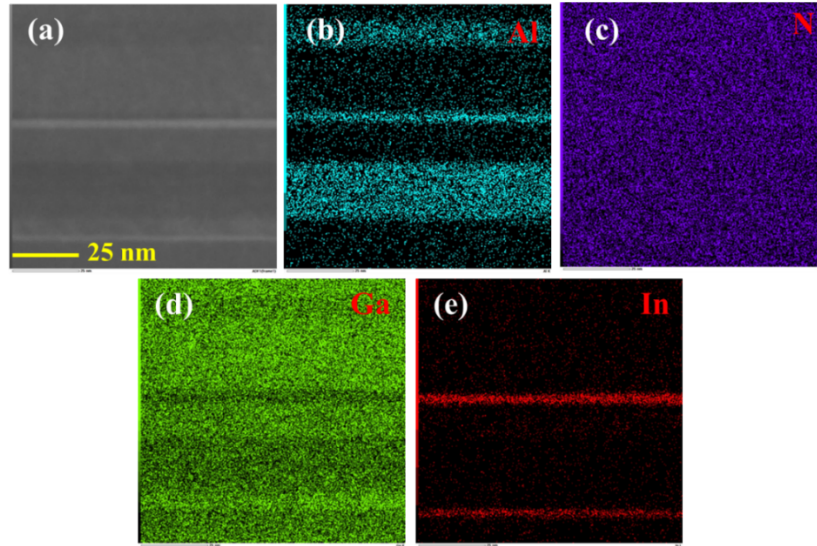


Fig. 3. (a) Cross-sectional STEM image of red single InGaN QW, (b-e) the elemental mappings of Al, N, Ga and In atoms distributed in the InGaN active region.

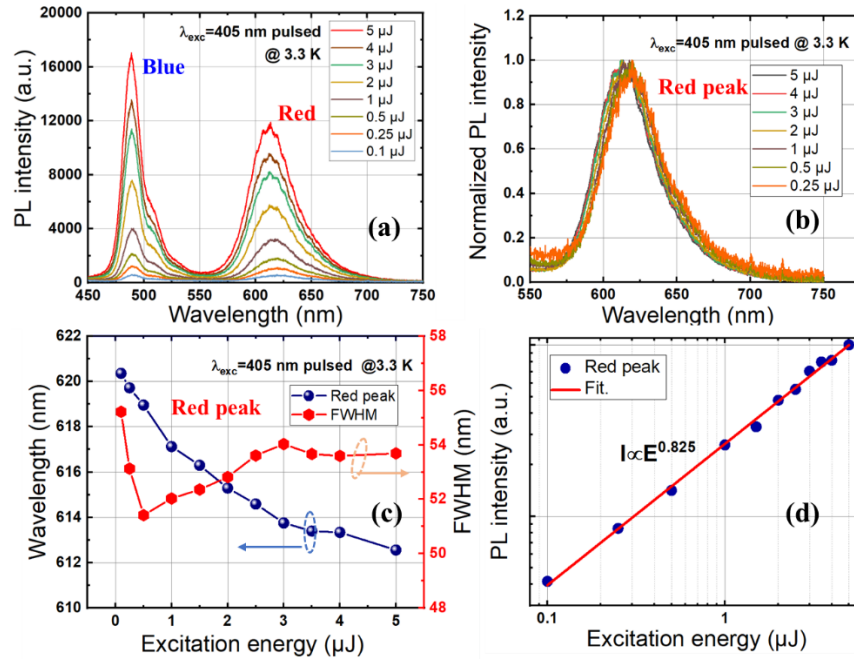


Fig. 4. At 3.3 K, (a) The measured PL spectra and (b) the normalized PL spectra of QW wafer at different excitation energies. (c) The wavelength and FWHM and (d) the integrated PL intensity of the red peak as a function of excitation energies.

of the excitation energy (E), it is confirmed that radiative recombination is the dominant carrier recombination process in the red QW at 3.3 K. And it is accompanied by Auger recombination at low temperature.

The fabrication process of the red InGaN microcavity is shown in Fig. 5. We used multi-pair $\text{TiO}_2/\text{SiO}_2$ dielectric DBRs as p-side and n-side mirrors. Step 1, multi-pair $\text{TiO}_2/\text{SiO}_2$ DBRs are grown on the surface of p-GaN epitaxial layer by electron beam evaporation technique. Step 2, the sample is transferred to a double-polishing sapphire substrate as a temporary support by bonding process. Step 3, the patterned sapphire substrate(PSS) is removed by Laser Lift-off(LLO) technology. Step 4, The n-side GaN layer is thinned and polished by chemical mechanical polishing(CMP). The u-GaN layer and part of the n-GaN layer are removed, until the desired cavity length. Step 5, the multiple-pair $\text{TiO}_2/\text{SiO}_2$ DBRs are grown on the polished surface as n-side mirror and complete the whole fabrication procedure.

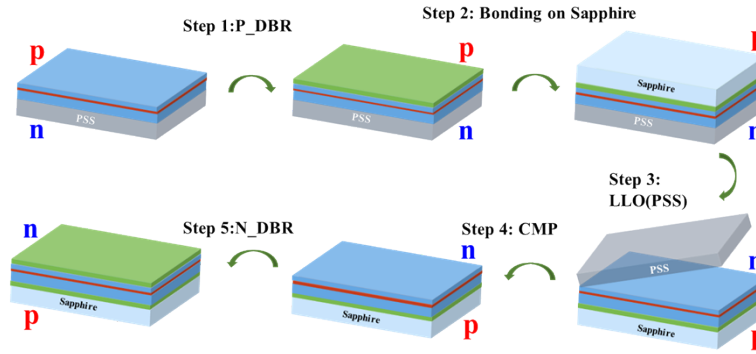


Fig. 5. Schematic of fabrication process of red InGaN microcavity.

After LLO, CMP is used to treat the surface and reduce the thickness of layer. The surface morphology of the sample was obtained by atomic force microscope(AFM) as shown in Fig. 6(a) and (b). AFM scans a random location with an area of $10\ \mu\text{m} \times 10\ \mu\text{m}$. From Fig. 6(a), the root mean square(RMS) roughness δ of the surface is 0.4 nm, which proves that CMP is beneficial to smooth the surface of the sample. The surface scattering loss α due to surface roughness can be obtained by the following formula [17]:

$$\alpha = A \left\{ 1 - \exp \left[- \left(\frac{4\pi\delta}{\lambda} \right)^2 \right] \right\} \quad (2)$$

where $A = 1.02$ is the correction coefficient, and λ is the corresponding wavelength of the standing wave in the resonator. The surface scattering loss α is estimated to be about 0.007%, being a pretty low value.

The polished sample is a half-cavity device, and PL measurements are performed on both n and p sides at room temperature(RT). A 405 nm continuous wave(CW) laser is used as the excitation source. As shown in Fig. 7(a), a strong emission peak at 450-500 nm can be clearly observed by n-side excitation. This phenomenon is attributed to the fact that the pumping laser must first pass through the blue QW. The strong emission peak of blue QW is unfavorable to the luminescence of the red microcavity. Therefore, in the rest of the work, the PL measurement with the same conditions on the p-side is performed. As shown in Fig. 7(b), The emission peak of the blue QW is significantly reduced. In terms of epitaxial structure, the p-side incident laser first arrives at the red QW and enhances the PL intensity of the red QW. From PL spectra of half-cavity devices, the advantage of p-side incidence and output is quite prominent.

According to the half-cavity PL spectrum, the central wavelength of n-side DBRs is designed to be around 630 nm. In order to facilitate the output of p-side in the microcavity, the reflectivity of the n-side DBRs is designed to be higher. By simulating 12 pairs of $\text{TiO}_2/\text{SiO}_2$ DBRs, the

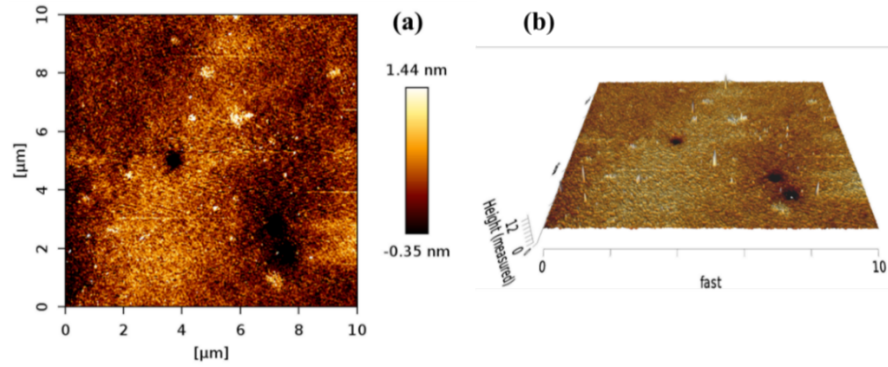


Fig. 6. (a) Planar view and (b) three-dimensional view of AFM of the polished sample surface after LLO.

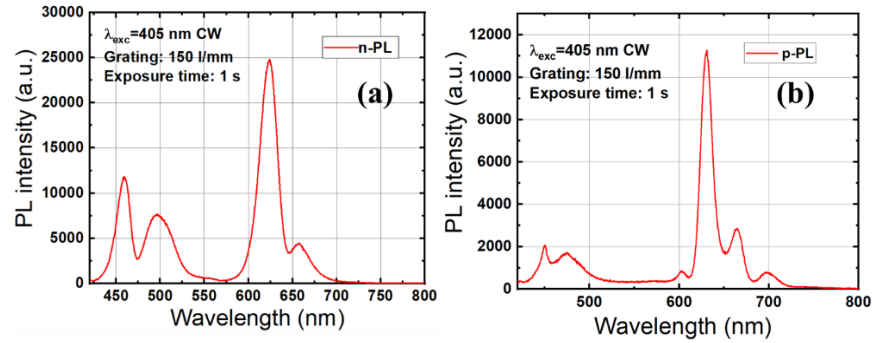


Fig. 7. PL spectra of the half cavity excited from (a) n side and (b) p side, respectively.

reflectivity can reach 99.99%. The stopband width covers 589-721 nm with the reflectance greater than 99.7%, as shown in Fig. 8.

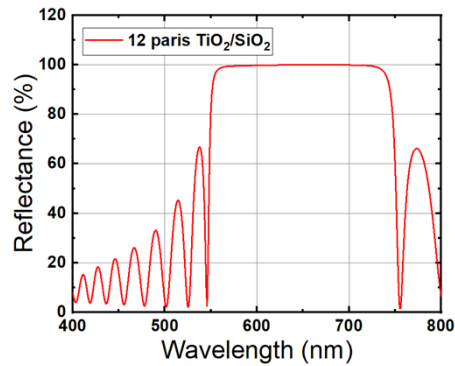


Fig. 8. The simulated reflectance of the 12-pair DBRs in n-side.

3. Characterization and discussion of microcavity

Using the same 405 nm CW laser as in half-cavity measurements, PL measurements of the full-cavity structure were performed on red InGaN microcavity at RT with p-side incidence. The

PL spectra of the red InGaN microcavity under different excitation power are shown in Fig. 9(a). Two cavity modes are observed at 587.7 and 612.3 nm, respectively. By the separation of modes, the effective cavity length of the red InGaN microcavity is calculated to be about 2372 nm [18,19]. By using this cavity length, the simulated cavity mode position of the whole cavity is shown in Fig. 9(b). Multiple cavity modes are known to appear at around 533, 557.6, 585, 613, 645 and 680 nm.

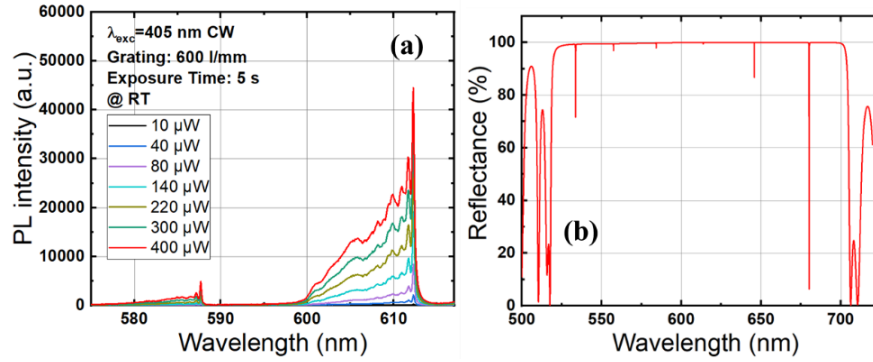


Fig. 9. The cavity modes of red InGaN microcavity: (a) experimental results and (b) simulated results.

The experimental results show that the emission of 612.3 nm is strongest. For this mode, the normalized PL spectra are shown in Fig. 10. It can be observed that the peak does not move and broaden with the change of excitation power. This phenomenon is significantly different from the emission characteristics of the epitaxial wafer, indicating the luminescence is strongly stabilized by the microcavity mode. In other words, microcavity is very effective in suppression of peak shift of optical devices under operation. This is because the emission peak is determined by the optical mode of the cavity, rather than the QW itself. So, it is not influenced by band filling and variation of QCSE inside the QW.

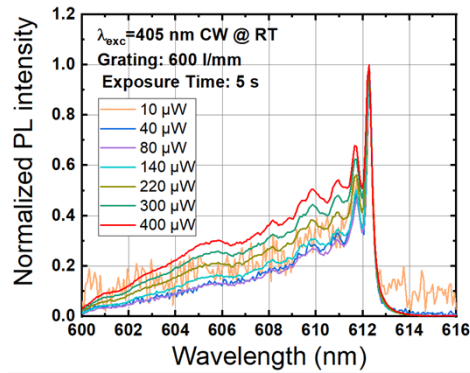


Fig. 10. The normalized PL spectra of red InGaN microcavity with different excitation power at 612.3 nm.

The quality of resonator can be quantitatively characterized by the quality factor(Q value). A good quality of the resonator can reduce the loss of periodic oscillation, resulting in the increase of Q value. The Q value can be calculated by the ratio of the peak wavelength and the

corresponding line width, as following formula [20,21]:

$$Q = \lambda / \delta\lambda \quad (3)$$

where $\delta\lambda$ is the line width of the cavity mode, λ is the wavelength at the cavity mode. The multi-order modes at 612.3 nm were fitted, as shown in Fig. 11. The peak wavelength, FWHM and calculated Q value of each peak were shown in Table 1. A narrow emission linewidth is ~ 0.26 nm at 612.3 nm, and the Q value of the cavity mode is about 2355. This is much larger than the Q values reported for red RCLEDs based on GaN:Eu, O and AlInGaP [11,12]. Together with our previous results of Q values [13], it can be concluded that the cavity quality of red InGaN microcavity is much better.

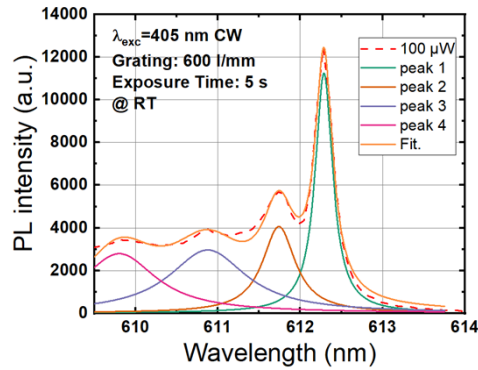


Fig. 11. The fitting of multi-order modes at 612.3 nm

Table 1. The peak wavelength, FWHM and calculated Q value of each peak

	Wavelength (nm)	FWHM (nm)	Q value
1 st	612.3	0.26	2355
2 nd	611.7	0.48	1274
3 rd	610.8	1.14	536
4 th	609.8	1.09	559

From Fig. 11, there are a few emission peaks on the higher energy side of the peak at 612.3 nm. The 612.3 nm peak is known as the longitudinal mode of the FP cavity while other peaks are the higher-order modes caused by lateral confinement effect on the optical mode in the cavity. In the orange-red InGaN based RCLEDs, the higher-order lateral modes at 602 nm were also observed where a lateral difference in the refractive index was intentionally introduced during fabrication [13]. In the present study, however, there is no such a lateral difference in the sample structure. So, the mechanism is different. When a semiconductor is optically excited above or close to an electronic transition, a change of the refractive index occurs due to the large carrier density. If the change is positive, light confinement will be possible [22,23]. Together with the FP cavity effect, three-dimensional confinement to the carriers is realized.

TRPL was further measured by using a 400 nm pulsed femtosecond laser as the excitation source with a self-built TRPL test system at RT and p-side incidence. By TRPL measurements, the carrier dynamics in microcavity and epitaxial wafer are compared and investigated. Figures 12(a) and (b) are TRPL images of epitaxial wafer and red InGaN microcavity at excitation power of 80 μ W. In Fig. 12(a), carrier recombination was observed at longer wavelength positions

(deep localization states) with increasing decay time. In Fig. 12(b), it can be clearly seen that the microcavity has a great influence on red emission. That is, the position of the emission is stabilized by the cavity mode. Figure 12(c) shows that the TRPL decay curves of wafer at a few emission wavelengths (585.9, 607.3, 628.8 and 655 nm, the same position as cavity modes in Fig. 12(d)). With the increase of wavelength, the carrier recombination time becomes longer. By a single exponential function fitting, the decay time of the epitaxial wafer is obtained in Table 2. The decay time is increasing with the red shift of wavelength, which is attributed to the carrier transferring from higher energy states to lower energy states of the localization centers [24].

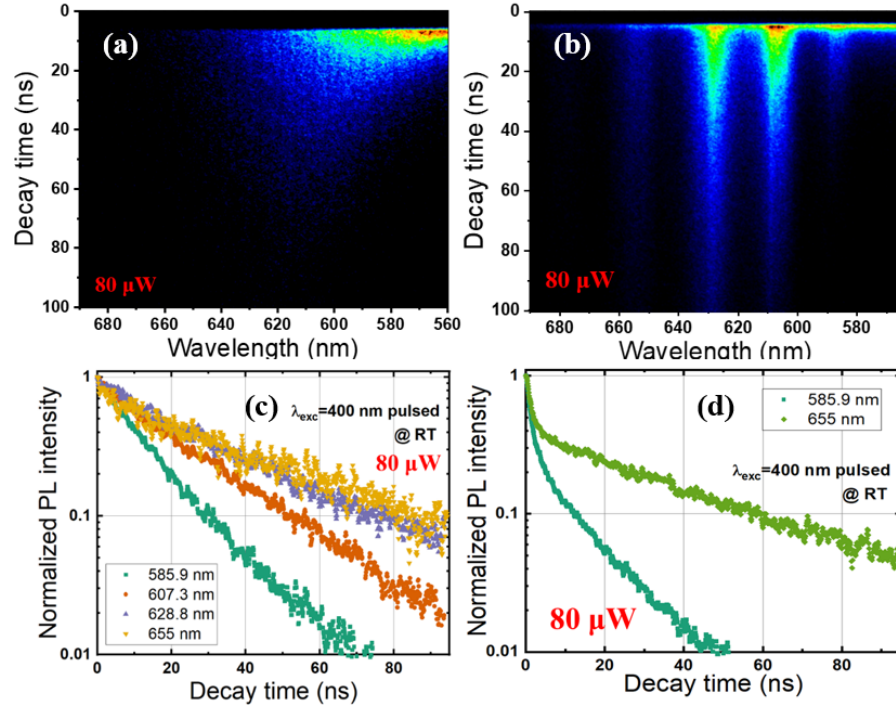


Fig. 12. (a) and (b) TRPL images of epitaxial red InGaN QW wafer and related microcavity at 80 μ W. (c) and (d) Decay curves at different wavelengths of QW and microcavity, respectively

Table 2. Decay times of cavity modes and QW wafer at 80 μ W

Cavity mode	Microcavity fast decay time(ns)	Microcavity slow decay time (ns)	Wafer decay time (ns)
585.9 nm	1.16	11.5	12.3
607.3 nm	1.36	17.5	21.7
628.8 nm	1.48	23.3	26.6
655 nm	1.27	37.4	32.5

Figure 12(d) shows the decay curves of the red InGaN microcavity at 585.9 and 655 nm cavity modes (for clarity, only two decay curves are displayed). Differing to the case of as-grown wafer, there are two decay components in a microcavity. By fitting TRPL decay curves at different cavity modes, the fast and slow decay times are obtained in Table 2. The slow decay time is similar to the results of the wafer, while the fast decay is newly appeared which is attributed to the

Purcell effect in a microcavity. Purcell effect increases the photon state density of cavity modes while suppressing the photon state density of other wavelengths, leading to the rapid radiation recombination of photogenerated carriers in cavity modes and the fast decay process occurs. The slow decay time of the red InGaN microcavity is consistent with that of the wafer, demonstrating that the slow decay process is almost unaffected by Purcell effect in microcavity, which shows that the slow decay is related to the transfer and recombination of carriers in deep localization states in red QW.

Since the Purcell factor is written as [25]:

$$F_P = \frac{\tau_{\text{free}}}{\tau_{\text{cav}}} = \frac{3Q(\lambda_c/n)^3}{4\pi^2 V_{\text{eff}}} \quad (4)$$

It is clear that, in order to enhance the Purcell effect, it is necessary to decrease the cavity length (proportional to volume) and/or increase the Q value (reduce the optical loss).

4. Conclusion

Optical properties of InGaN/GaN red QW and their microcavities were studied and compared under optical pumping. Incidence configuration of the excitation laser from the p-side was employed for both samples in order to acquire better emission characteristics. The good quality of the QW wafer was confirmed by X-ray, STEM and PL measurements. The design and fabrication processes of red InGaN microcavity were described in detail. A high-quality microcavity with Q value of 2355 was realized at the longitudinal mode of 612.3 nm. The lateral confinement on the photons in the microcavity was explained by a change in the refractive index of the laser-irradiation area because of the increase of carrier density, resulting in discrete higher-order modes. It was found that the Purcell effect accelerates the radiation recombination rate, leading to the fast decay process in the red InGaN microcavity which does exist for QWs only. The microcavity makes the red emission more pure and more stable. These results lay a foundation for the realization of InGaN-based red VCSELs in the future.

Funding. National Natural Science Foundation of China (U21A20493, 62234011).

Acknowledgments. The authors would like to thank Ya-Chao Wang, Zhi-Wei Zheng and Hao Long of Xiamen University for support and useful discussions.

Disclosures. The authors declare no conflicts of interest.

Data availability. Data underlying the results presented in this paper are not publicly available at this time but may be obtained from the authors upon reasonable request.

References

1. Y. Yamashita, H. Tamura, N. Horio, *et al.*, "Control of emission wavelength of GaInN single quantum well, light emitting diodes grown by metalorganic chemical vapor deposition in a split-flow reactor," *Jpn. J. Appl. Phys.* **42**, 4197–4202 (2003).
2. Z. Zhuang, D. Iida, M. Velazquez-Rizo, *et al.*, "606-nm InGaN Amber Micro-Light-Emitting Diodes With an On-Wafer External Quantum Efficiency of 0.56%," *IEEE Electron Device Lett.* **42**(7), 1029–1032 (2021).
3. T. Mukai, M. Yamada, S. Nakamura, *et al.*, "Characteristics of InGaN-based UV/blue/green/amber/red light-emitting diodes," *Jpn. J. Appl. Phys.* **38**(7R), 3976–3981 (1999).
4. Y. J. Zhao, S. H. Oh, F. Wu, *et al.*, "Green Semipolar (20 $\bar{2}$ 1) InGaN Light-Emitting Diodes with Small Wavelength Shift and Narrow Spectral Linewidth," *Appl. Phys. Express* **6**, 062102 (2013).
5. X. Hou, S.-S. Fan, H. Xu, *et al.*, "Optical properties of InGaN-based red multiple quantum wells," *Appl. Phys. Lett.* **120**(26), 1 (2022).
6. A. L. Holsteen, Søren Raza, P. Fan, *et al.*, "Purcell effect for active tuning of light scattering from semiconductor optical antennas," *Science* **358**(6369), 1407–1410 (2017).
7. E. M. Purcell, "Spontaneous Emission Probabilities at Radio Frequencies," in *Confined Electrons and Photons: New Physics and Applications*, E. Burstein and C. Weisbuch, eds. (Springer US, Boston, MA, 1995), pp. 839.
8. J. H. Kim, T. Cai, C. J. K. Richardson, *et al.*, "Two-photon interference from a bright single-photon source at telecom wavelengths," *Optica* **3**(6), 577–584 (2016).

9. C. M. Lee, M. A. Buyukkaya, S. Harper, *et al.*, "Bright Telecom-Wavelength Single Photons Based on a Tapered Nanobeam," *Nano Lett.* **21**(1), 323–329 (2021).
10. J. Vuckovic, D. Englund, D. Fattal, *et al.*, "Generation and manipulation of nonclassical light using photonic crystals," *Phys. E* **32**(1-2), 466–470 (2006).
11. T. Inaba, J. Tatebayashi, K. Shiomi, *et al.*, "Ga_N:Eu,O-Based Resonant-Cavity Light Emitting Diodes with Conductive AlInN/GaN Distributed Bragg Reflectors," *ACS Appl. Electron. Mater.* **2**(3), 732–738 (2020).
12. M. M. Dumitrescu, M.J. Saarinen, M.D. Guina, *et al.*, "High-speed resonant cavity light-emitting diodes at 650 nm," *IEEE J. Sel. Top. Quantum Electron.* **8**(2), 219–230 (2002).
13. W. Ou, Y. Mei, D. Iida, *et al.*, "InGa_N-Based Orange-Red Resonant Cavity Light-Emitting Diodes," *J. Lightwave Technol.* **40**(13), 4337–4343 (2022).
14. D. Iida, Z. Zhuang, P. Kirilenko, *et al.*, "633-nm InGa_N-based red LEDs grown on thick underlying Ga_N layers with reduced in-plane residual stress," *Appl. Phys. Lett.* **116**(16), 1 (2020).
15. X. Hou, S. Fan, D. Iida, *et al.*, "Photoluminescence of InGa_N-based red multiple quantum wells," *Opt. Express* **29**(19), 30237–30243 (2021).
16. Z. M. Zheng, Y. Mei, H. Long, *et al.*, "AlGa_N-Based Deep Ultraviolet Vertical-Cavity Surface-Emitting Laser," *IEEE Electron Device Lett.* **42**(3), 375–378 (2021).
17. Z. Gacevic, G. Rossbach, R. Butté, *et al.*, "Q-factor of (In,Ga)_N containing III-nitride microcavity grown by multiple deposition techniques," *J. Appl. Phys.* **114**(23), 1 (2013).
18. G. B. Lin, D.-Y. Kim, Q. Shan, *et al.*, "Effect of quantum barrier thickness in the multiple-quantum-well active region of GaInN/GaN light-emitting diodes," *IEEE Photonics J.* **5**, 1600207 (2013).
19. T. Onishi, O. Imafuji, K. Nagamatsu, *et al.*, "Continuous wave operation of Ga_N vertical cavity surface emitting lasers at room temperature," *IEEE J. Quantum Electron.* **48**(9), 1107–1112 (2012).
20. M. Arita, S. Kako, S. Iwamoto, *et al.*, "Fabrication of AlGa_N Two-Dimensional Photonic Crystal Nanocavities by Selective Thermal Decomposition of Ga_N," *Appl. Phys. Express* **5**, 126502 (2012).
21. C.-C. Lin and C.-T. Lee, "Ga_N-based resonant-cavity light-emitting diodes with top and bottom dielectric distributed Bragg reflectors," *IEEE Photonics Technol. Lett.* **22**(17), 1291–1293 (2010).
22. S. Anguiano, A. A. Reynoso, A. E. Bruchhausen, *et al.*, "Three-dimensional trapping of light with light in semiconductor planar microcavities," *Phys. Rev. B* **99**(19), 195308 (2019).
23. S. Schmittrink, D. S. Chemla, D. A. B. Miller, *et al.*, "Theory of transient excitonic optical nonlinearities in semiconductor quantum well structures," *Phys. Rev. B* **32**, 6601–6609 (1985).
24. X. Hou, T. Yang, S.-S. Fan, *et al.*, "Improvement of optical properties of InGa_N-based red multiple quantum wells," *Opt. Express* **31**(11), 18567–18575 (2023).
25. M. Agio and D. M. Cano, "Nano-optics: The Purcell factor of nanoresonators," *Nat. Photonics* **7**(9), 674–675 (2013).